Chapter 3

Chemistries for Patterning Robust DNA Microbarcodes Enable Multiplex Assays of Cytoplasm Proteins from Single Cancer Cells

3.1 Introduction

The demand for parallel, multiplex analysis of protein biomarkers from ever smaller biospecimens is an increasing trend for both fundamental biology and clinical diagnostics.[1–3] The most highly multiplex protein assays rely on spatially encoded antibody microarrays,[4–6] and small biospecimen samples are now routinely manipulated using microfluidics approaches. The integration of antibody microarray techniques with microfluidic chips has only been explored relatively recently. One challenge arises from the relative instability of antibodies to microfluidics fabrication conditions. In recent years, several groups have devised methods to transform standard DNA microarrays *in situ* into protein microarrays and cell-capture platforms.[7–13] These approaches capitalize on the chemical robustness of DNA oligomers, and the reliable assembly of DNA-labeled structures via complementary hybridization. Recently, Fan et al. utilized a microfluidics-based flow patterning technique to generate DNA barcode-type arrays at 10× higher density than standard, spotted microarrays.[15] The DNA barcodes were converted into antibody arrays using the DNA-Encoded Antibody Library (DEAL) technique, and then applied towards the measurement of a highly multiplex panel of proteins from a pinprick of whole blood.

A second challenge involves scaling such miniaturized DNA microarrays so that a large surface area can be encoded. This problem is non-trivial, as it involves identifying chemistries for patterning 10^{-5}-m-wide, 1-m-long strips of biomolecules with a uniformity that permits those patterns to be utilized in hundreds to thousands of quantitative protein assays per chip. Here, we explore the surface chemistry associated with a microfluidics-based flow patterning of DNA barcodes, with an eye towards producing highly reproducible and robust barcodes. We then apply the optimized chemistry towards assaying a panel of cytoplasmic proteins from single cells.

3.2 Experimental Methods

3.2.1 Microfluidic chip fabrication for DNA patterning

Microfluidic-patterning PDMS chips were fabricated by soft lithography. The master mold was prepared using either a negative photoresist, SU8 2010, with photolithography, or an etched silicon mold generated by a deep reactive ion etching (DRIE) process. The mold has long meandering channels with a 20×20 μm cross section. The distance from channel to channel is also 20 μm, which generates 10× higher density than standard, spotted microarrays. Sylgard PDMS (Corning) prepolymer and curing agent were mixed in a 10:1 ratio (w/w), poured onto the mold, and cured (80°, 1 h). The cured PDMS slab was released from the mold, inlet/outlet holes were punched, and the device was bonded onto a PLL coated (C40-5257-M20, Thermo scientific) or aminated glass slide (48382-220, VWR) to form enclosed channels. The number of microfluidic channels determines the size of the microarray; 13 parallel microchannels were used in this study.

3.2.2 Patterning of DNA barcode arrays

For the DNA filling test, a 30 mer DNA oligomer labeled with Cy3 fluorescence tag on the 5’ end (5’-/Cy3/-AAA AAA AAA ATA CGG ACT TAG CTC CAG GAT - 3') in a 1:1

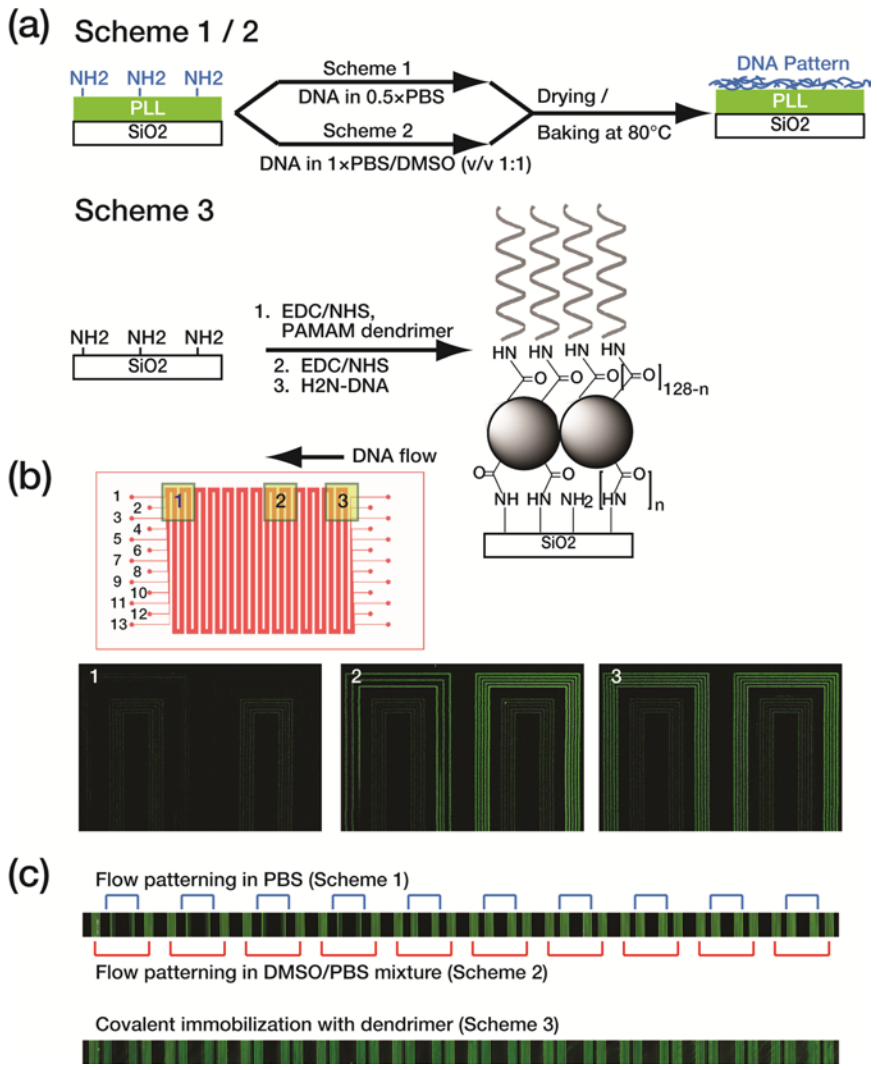

Figure 3.1 (a) Surface treatment schemes. (b) Design of the DNA patterning device (top) and fluorescence image of DNAs filled into the channel (still in solution). Outer five channels are filled with DNAs in 1:1 mixture of PBS and water (Scheme 1). Inner five channels are filled with DNAs in 1:1 mixture of PBS and DMSO (Scheme 2). Three channels in between are left empty for visualization. (c) Fluorescence images of patterned DNAs by three schemes

mixture (v/v) of 1×PBS buffer and DMSO or a 1:1 mixture (v/v) of 1×PBS buffer and deionized (DI) water was used. The final DNA concentration was 2.5 μM. DNA solution was pushed into the channel under a constant pressure (2.5 psi). Immediately after the channels were fully filled, fluorescence images were obtained by confocal microscopy.

Dendrimer-based microarrays were prepared using aminated substrates. Generation 4.5 Poly(amidoamine) (PAMAM) dendrimers (470457-2.5G, Aldrich), 5% wt in MeOH, were mixed 1:1 (v/v) with EDC/NHS (0.2 M) in MES buffer (0.1 M, pH 6.0). After 5 minutes of incubation, the activated dendrimers were introduced to the microfluidic channels, and allowed to flow (2 h). Following a brief MeOH rinse to remove unbound dendrimers, the channels were filled with EDC/NHS (0.2 M) in MES (0.1 M, pH 5.3) with NaCl (0.5 M). After 0.5 h, 5’ aminated DNA sequences in 1×PBS (200 μM) were introduced to the channels and allowed to flow (2 h). Thereafter, the microfluidic device was removed from the substrate, and the latter was rinsed copiously with DI water. Prepared substrates that were not used immediately were stored in a desiccator.

To generate the DNA barcode array for multi-protein detection and single cell lysis test, 13 orthogonal DNA oligomer solutions (sequences are provided in Table 3.1) in 1×PBS buffer (400 μM) were mixed with DMSO (in 1:2 ratio, v/v) and flowed into each of the microfluidic channels (Scheme 3.2). For Scheme 3.1, DNA solutions in 1×PBS buffer were used. The DNA-filled chip was placed in a desiccator until the solvent evaporated completely, leaving only DNA molecules behind. Finally, the PDMS elastomer was removed from the glass substrate and the microarray-patterned DNAs were cross-linked to the PLL by thermal treatment (80 °C, 4 h). The slide was gently rinsed with DI water prior to use in order to remove salt crystals remaining from the solution evaporation step.

Table 3.1 Sequences and terminal functionalization of oligonucleotides: All oligonucleotides were synthesized by Integrated DNA Technology (IDT) and purified via high-performance liquid chromatography (HPLC). The DNA coding oligomers were pre-tested for orthogonality to ensure that cross-hybridization between non-complementary oligomer strands was negligible (< 1% in photon counts).

Name	Sequence	Melting Point
A	5'- AAA AAA AAA AAA AAT CCT GGA GCT AAG TCC GTA-3'	57.9
A'	5' NH3- AAA AAA AAA ATA CGG ACT TAG CTC CAG GAT-3'	57.2
B	5'-AAA AAA AAA AAA AGC CTC ATT GAA TCA TGC CTA -3'	57.4
B'	5' NH3AAA AAA AAA ATA GGC ATG ATT CAA TGA GGC -3'	55.9
C	5'- AAA AAA AAA AAA AGC ACT CGT CTA CTA TCG CTA -3'	57.6
C'	5' NH3-AAA AAA AAA ATA GCG ATA GTA GAC GAG TGC -3'	56.2
D	5'-AAA AAA AAA AAA AAT GGT CGA GAT GTC AGA GTA -3'	56.5
D'	5' NH3-AAA AAA AAA ATA CTC TGA CAT CTC GAC CAT -3'	55.7
E	5'-AAA AAA AAA AAA AAT GTG AAG TGG CAG TAT CTA -3'	55.7
E'	5' NH3-AAA AAA AAA ATA GAT ACT GCC ACT TCA CAT -3'	54.7
F	5'-AAA AAA AAA AAA AAT CAG GTA AGG TTC ACG GTA -3'	56.9
F'	5' NH3-AAA AAA AAA ATA CCG TGA ACC TTA CCT GAT -3'	56.1
G	5'-AAA AAA AAA AGA GTA GCC TTC CCG AGC ATT-3'	59.3
G'	5' NH3-AAA AAA AAA AAA TGC TCG GGA AGG CTA CTC-3'	58.6
H	5'-AAA AAA AAA AAT TGA CCA AAC TGC GGT GCG-3'	59.9
H'	5' NH3-AAA AAA AAA ACG CAC CGC AGT TTG GTC AAT-3'	60.8
I	5'-AAA AAA AAA ATG CCC TAT TGT TGC GTC GGA-3'	60.1
I'	5' NH3-AAA AAA AAA ATC CGA CGC AAC AAT AGG GCA-3'	60.1
J	5'-AAA AAA AAA ATC TTC TAG TTG TCG AGC AGG-3'	56.5
J'	5' NH3-AAA AAA AAA ACC TGC TCG ACA ACT AGA AGA-3'	57.5
K	5'-AAA AAA AAA ATA ATC TAA TTC TGG TCG CGG-3'	55.4
K'	5' NH3-AAA AAA AAA ACC GCG ACC AGA ATT AGA TTA-3'	56.3
L	5'-AAA AAA AAA AGT GAT TAA GTC TGC TTC GGC-3'	57.2
L'	5' NH3-AAA AAA AAA AGC CGA AGC AGA CTT AAT CAC-3'	57.2
M	5'-Cy3-AAA AAA AAA AGT CGA GGA TTC TGA ACC TGT-3'	57.6
M'	5' NH3-AAA AAA AAA AAC AGG TTC AGA ATC CTC GAC-3'	56.9

3.2.3 Microfluidic chip fabrication for multi-protein detection

The PDMS microfluidic chip for the cell experiment was fabricated by two-layer soft lithography.[16] A push-down valve configuration was utilized with a thick control layer bonded together with a thin flow layer. The molds for the control layer and the flow layer were fabricated with SU8 2010 negative photoresist (~ 20 μm thickness) and SPR 220

positive photoresist (~ 18 μm), respectively. The photoresist patterns for the flow layer were rounded via thermal treatment. The thick control layer was molded with a 5:1 mixture of GE RTV 615 PDMS prepolymer part A and part B (w/w) and the flow layer was formed by spin-coating a 20:1 mixture of GE RTV 615 part A and part B (w/w) on the flow layer mold (2000 rpm, 60 sec). Both layers were cured (80°C, 1 h), whereupon the control layer was cut from its mold and aligned to the flow layer. An additional thermal treatment (80°C, 1 h) ensured that the two layers bonded into a monolithic device, which was then peeled from its mold and punched to create appropriate access holes. Finally, the PDMS chip was thermally bonded to the DNA microbarcodes-patterned glass slide to form the working device.

3.2.4 Cell culture

The human GBM cell line U87 was cultured in DMEM (American Type Culture Collection, ATCC) supplemented with 10% fetal bovine serum (FBS, Sigma-Aldrich). U87 cells were serum-starved for 1 day and then stimulated by EGF (50 ng/ml, 10 min) before they were introduced into the device.

3.2.5 Multi-protein detection

Protein detection assays were initiated by blocking the chip with 3% bovine serum albumin (BSA) in PBS to prevent non-specific binding. This 3% BSA/PBS solution was used as a working buffer for most subsequent steps. After blocking, a cocktail containing all 11 (Scheme 3.2) or 3 (Scheme 3.3) DNA-antibody conjugates (~ 0.5 μg/ml, 100 μl) in working buffer was flowed through the micro channels for 1 h. The unbound DNA-

antibody conjugates were washed away with fresh buffer. Then, target proteins were flowed through the microfluidic channels for 1 h. These were followed by a 200 μl cocktail containing biotin-labeled detection antibodies (~ 0.5 μg/ml) in working buffer, and thereafter a 200 μl mixture of 1 μg/ml Cy5-labeled streptavidin and 25 nM Cy3-labeled M' ssDNA in working buffer to complete the immune sandwich assay. DNA sequence M is used for a location reference. The microchannels were rinsed with working buffer once more before the PDMS chip was removed; the bare microarray slide was rinsed sequentially with 1×PBS, 0.5×PBS, DI water, and was finally subjected to spin-drying.

3.2.6 On-chip cell lysis and mulplexed intracellular protein profiling from single cells

The multi-protein detection procedure described above was slightly modified for intracellular protein profiling experiments. Again, the chip was initially blocked with a 3% BSA/PBS working buffer, followed by a 200 μl cocktail containing all 11 DNA-antibody conjugates (~ 0.5 μg/ml, Table 3.2) in working buffer (continuously flowed for 1 h). Unbound DNA-antibody conjugates were washed off with fresh buffer. The lysis buffer (Cell Signaling) was loaded into the lysis buffer channels while the valve 1 (V1 in Fig. 3.9a) was kept closed by applying 15–20 psi constant pressure. Then cells were introduced to the cell loading channels and microfluidic valves (V2 in Fig. 3.9a) were closed by applying 15–20 psi constant pressure; this converts the 8 channels into 120 isolated microchamber sets. After cell numbers were counted under microscope, V1 valves were released to allow diffusion of lysis buffer to the neighboring microchamber containing different numbers of cells. The cell lysis was performed on ice for two h. After that, the V2 valves were

Table 3.2 Summary of antibodies used for cell lysis experiments: All antibody pairs except p-VEGFR2 were purchased as ELISA kits of R&D systems (DuoSet® Elisa Development Reagents) containing capture antibodies, biotinylated detection antibodies, and standard proteins. Capture antibodies bind both phosphorylated and unphosphorylated proteins. The biotinylated detection antibodies detect only the phosphorylated variants of the proteins. VEGFR2 capture antibody, and p-VEGFR2 (Y1214) detection antibodies were purchased from Abcam.

DNA label	Antibody	Source
A’	Human p-PDGFR□ (Y751) kit	R&D DYC3096
B’	Human p-Src (Y419) kit	R&D DYC2685
C’	Human p-mTOR (S2448) kit	R&D DYC1665
D’	Human p-p70S6K (T389) kit	R&D DYC896
E’	Human p-GSK3α/β (S21/S9) kit	R&D DYC2630
G’	Human p-p38 α (T180/Y182) kit	R&D DYC869
H’	Human p-ERK (T202/Y204) kit	R&D DYC1825
I’	Human p-JNK2 (T183/Y185) kit	R&D DYC2236
K’	Human total EGFR kit	R&D DYC1854
L’	Human total P53 kit	R&D DYC1043
J’	Capture antibody: rabbit anti-human p-VEGFR2 (Y1214)	Abcam ab31480
	Detection antibody: biotin-labeled mouse anti-human VEGFR2	Abcam ab10975

released and the unbound cell lysate was quickly removed by flowing the fresh buffer. Then, a cocktail containing biotin-labeled detection antibodies (~ 0.5 μg/ml, 200 μl) in working buffer was flowed into the chip for 1 h on ice, followed by flowing a 200 μl mixture of Cy5-labeled straptavidin (1 μg/ml) and Cy3-labeled M’ ssDNA (25 nM) in working buffer to complete the sandwich immunoassay. Finally, the microchannels were

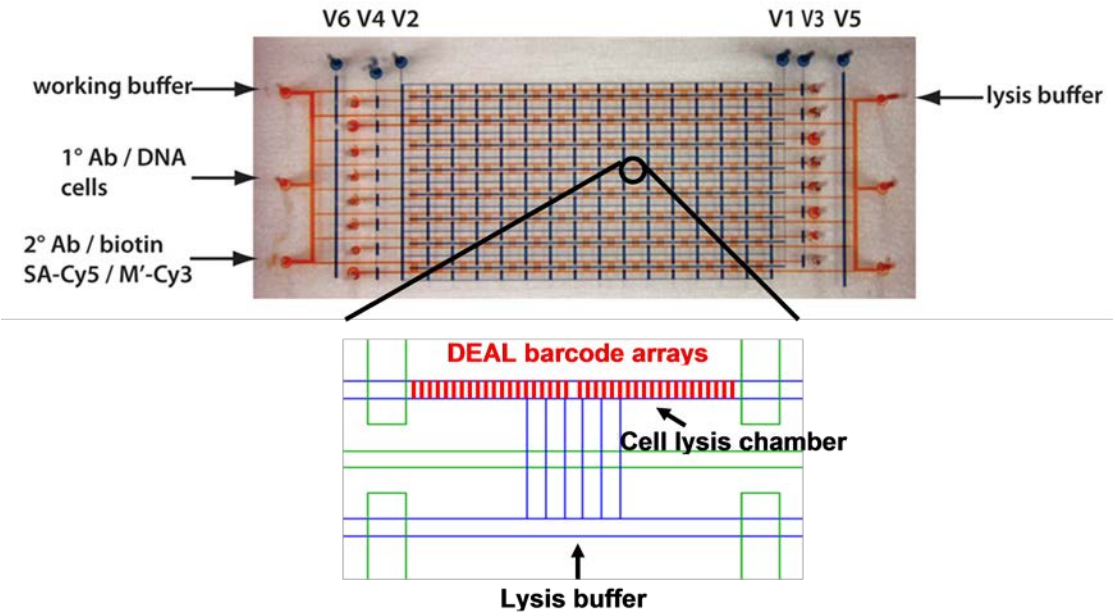

Figure 3.2 The Single-Cell Barcode Chip (SCBC) utilized for on-chip cell lysis and multiplex intracellular protein detection. V1 to V6 represent valves. V1 is used to control the diffusion of the cell lysis buffer to the cell lysis chamber, and closure of V2 results in the formation of isolated chambers from the long channels. V3, V4, V5, and V6 are utilized to control solution flows in the microchannels. Food dyes are used here to visualize the flow channels and control valves. The volume of each microchamber is ~ 2 nL.

rinsed with working buffer, the PDMS chip was removed, and the bare microarray slide was rinsed sequentially with 1×PBS, 0.5×PBS, and DI water, before spin-drying. The layout of the chip and used inlets for different solutions are described in Fig. 3.2.

3.2.7 Data analysis

The microarray slide was scanned with the GenePix 200B (Axon Instruments) to obtain a fluorescence image of both Cy3 and Cy5 channels. All scans were performed with the same setting of 50% (635 nm) and 15% (532 nm) laser power, 500 (635 nm) and 450 (532

nm) optical gain. The averaged fluorescence intensities for all barcodes in each chamber were obtained and matched to the cell number by custom-developed Excel or MATLAB codes.

3.2.8 Molecular dynamic simulation

The MD simulations were performed with the all-atom AMBER2003 force field[17, 18] using the Large-scale Atomic/Molecular Massively Parallel Simulator (LAMMPS) code.[19] As an initial structure, a single-strand DNA (5'-ACCCATGGAGCATTCCGGG-3') whose base pairs are randomly chosen was built using the Namot2 program.[20] Near the DNA strand, 19 sodium counter ions were included to neutralize the negatively charged 19 phosphate groups on the DNA backbone. Then this was immersed in a solvation box composed of either 1) 5206 water molecules + 106 DMSO molecules or 2) only 5206 water molecules. We used a TIP4P model to describe the water interactions.[21] We performed 3 ns NPT MD simulations using Nose-Hoover thermostat with a damping relaxation time of 0.1 ps and Andersen-Hoover barostat with a dimensionless cell mass factor of 1.0. The last 1 ns trajectory is employed for the analysis. To compute the electrostatic interactions, the particle-particle particle-mesh method[22] was employed using an accuracy criterion of 10^{-4}.

3.2.9 Modeling of electrostatic adsorption of DNA to poly-L-lysine (PLL) surface

This modeling follows the approach used in reference 22. [23]

The following assumptions are used for the simulation:

—Nonspecific DNA adhesion to the PDMS surface is insignificant compared with the adhesion to the PLL surface

—DNAs are instantaneously and irreversibly captured to the PLL surface when they are transported to the surface.

We start with the following mass transport equation,

$$v_x \frac{\partial C}{\partial x} = D \frac{\partial^2 C}{\partial y^2}$$

where v_x is the fluid velocity along the channel and y is the channel height. We can apply boundary conditions such that at the top and side walls, there are no concentration gradients.

In a rectangular channel the mass diffusion coefficient can be approximated by

$$h_{diff} = 3.81 \frac{D}{d_h}$$

where h_{diff} is the hydraulic channel diameter, $\frac{4\,[\text{cross-section area}]}{[\text{perimeter}]}$.

As DNA flows down the channel during the initial filling step, DNA is electrostatically captured by PLL on the surface, causing a concentration gradient. Thus, the mean concentration of the sample at position x, C_x can be expressed as

$$C_x = C_i e^{-h_{diff}\, w\, x/Q}$$

where C_i is the sample concentration at the channel entrance.

We are interested in how C_x changes as the sample flows along the channel and we can simply apply the parameters of our system.

It has been reported that the diffusion coefficients of labeled single-strand DNA are predicted by:

$$D_{label} = 4 \times 10^{-6} B^{-0.539}$$

where B is the number of bases.[24, 25]

In order to calculate C_x, we need the flow velocity. We measured the DNA sample filling speed (Fig. 3.6a) and used 536 μm/sec for simulation.

3.3 Results and Discussion

The microfluidics flow patterning chip is comprised of a patterned polydimethylsiloxane (PDMS) layer adhered to an aminated or PLL-coated glass substrate that provides the base surface for the microchannels. The microchannels are long (about 55 cm), meandering channels that span ~ 1.5 in^2 of our substrate, and are used to pattern a

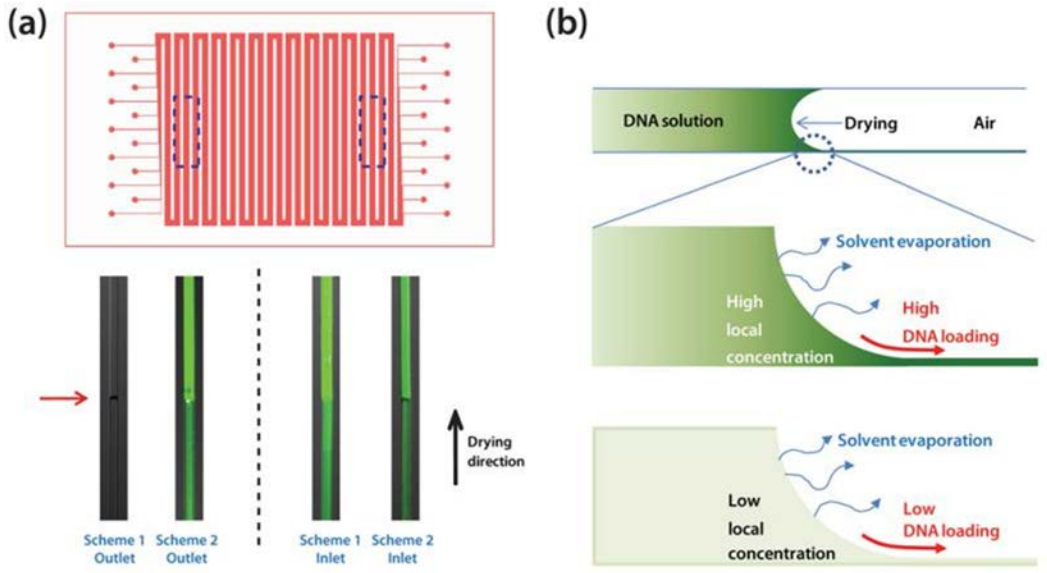

Figure 3.3 The microfluidic flow-patterning process to form the DNA barcodes. As the solvent evaporates through the PDMS elastomer, the concentration of the DNA oligomer solution increases. The oligomers are eventually deposited on the microchannel surfaces. **(**a) Fluorescence images of DNA solutions during the drying process for Schemes 1 and 2, in the region of the receding meniscus, and near the outlet (left) and inlet (right) sides of the microchannel. Note that, at the inlet side, the fluorescence intensity near the receding meniscus is very high – evidence of the high local concentration of DNA due to solvent evaporation. The channel filled according to Scheme 1 exhibits no significant DNA near the channel outlet due to excessive electrostatically-driven depletion near the inlet side. The red arrow indicates the location of the meniscus. (b) Schematics for the drying process with different local concentrations. A high local concentration is required to achieve suitable DNA loading on the substrate.

DNA barcode over most of the glass surface (Fig. 3.1b). After the flow patterning is completed, the PDMS layer is replaced with a second micropatterned PDMS layer that is designed to support a biological assay, such as the previously reported blood proteomics chip,[15] or the single-cell proteomics chips utilized here. For the microfluidic patterning method to be useful, it must generate a DNA barcode that exhibits high and uniform DNA loading over the entire substrate. We evaluated the patterning chemistries illustrated in Fig. 3.1a, Schemes 1-3. Schemes 3.1 and 3.2 are drawn from the conventional protocol for pin-spotted microarrays— a solution containing the DNA is introduced, the solvent is evaporated, and subsequent thermal or UV treatment is employed to cross-link the deposited DNA to the substrate. Scheme 3.1 utilizes ssDNA oligomers dissolved in phosphate buffered saline (PBS), whereas Scheme 3.2 employs ssDNAs in a 1:1 mixture of 1×PBS and dimethyl sulfoxide (DMSO). DMSO is used in conventional microarray preparation to improve feature consistency by reducing the rate of solvent evaporation and by denaturing the DNA[26] although, as described below, its role in this process is different. Scheme 3.3 utilizes a covalent immobilization method based upon a dendrimer scaffold.[27] Poly(amidoamine) (PAMAM) dendrimers (generation 4.5, carboxylate surface) have previously shown promise as DNA and protein microarray substrates. Dendrimers do not form entangled chains[28] and because harsh crosslinking procedures are avoided, dendrimer-immobilized DNA retains high accessibility and activity in microarray applications. Moreover, the highly branched structure of the dendrimers provides a high density of reactive sites for surface attachment and for DNA coupling, thus leading to a high overall binding capacity. For all cases, a high level of DNA loading has been shown to decrease non-specific binding when compared to standard microarray substrates.[11, 29–31]

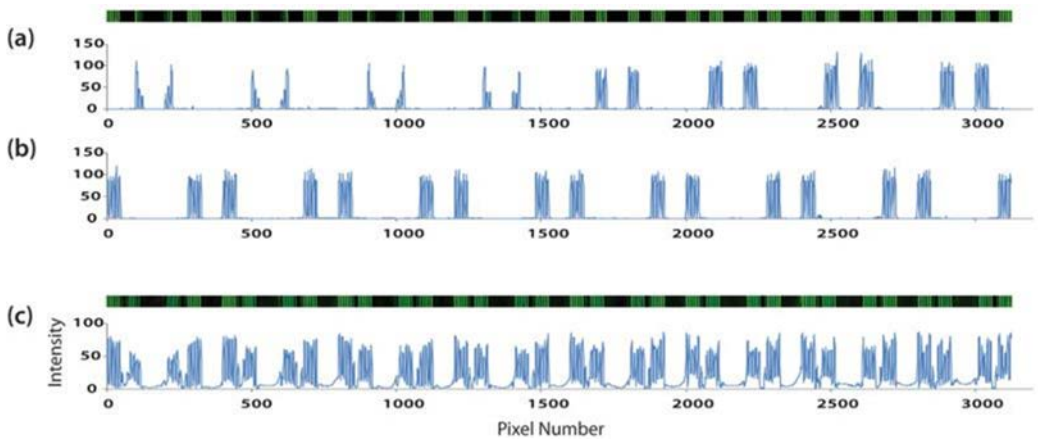

Figure 3.4 Line profiles for the DNAs patterned by Scheme 1 (a), Scheme 2 (b), and Scheme 3 (c). Y-axis is the intensity of the signal and x-axis is the pixel numbers. One pixel corresponds to 5 μm.

Fig. 3.1b (top) shows the PDMS chip design used for barcode patterning; 13 discrete channels (for a 13-element barcode) allow for a multiplex microarray. We loaded five adjacent channels according to Scheme 3.1, skipped three channels, and then loaded the remaining five channels according to Scheme 3.2. The use of fluorescently-tagged DNA permitted measurements of the DNA distribution within each individual channel immediately after introducing the solutions. Fig. 3.1b demonstrates a clear difference in aqueous DNA distribution across the chip: DNA loaded according to Scheme 3.1 (outer 5 channels) is notably lower in concentration near the middle of the chip (Fig. 3.1b, Region 2) and is barely detectable near the channel exit (Fig. 3.1b, Region 1). Conversely, DNA loaded according to Scheme 3.2 (inner 5 channels) presents an even, consistent distribution across the entire chip. Notably, Scheme 3.1 yields a relatively higher fluorescence intensity at the input side of the chip. These results clearly indicate that, for Scheme 3.1, the ssDNA oligomers are accumulating upstream during the early stages of flow, and so are depleted from the advancing solution by the time it reaches mid-chip. The actual patterning of the

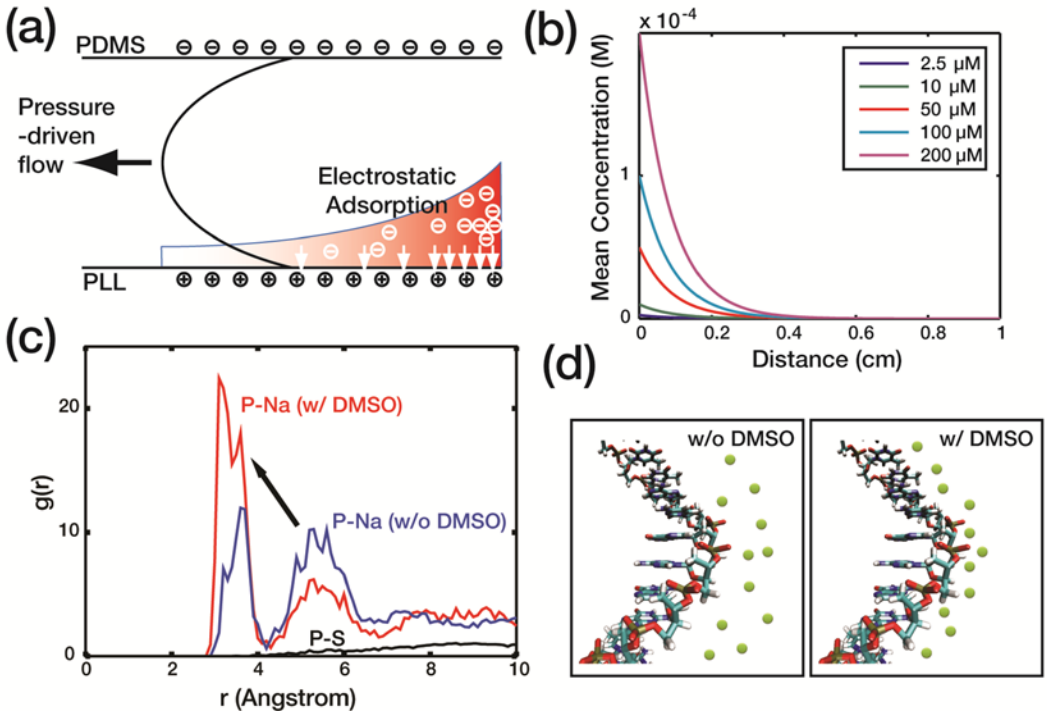

Figure 3.5 Electrostatic adsorption of DNAs on PLL surface and DMSO effect. (a) Schematic figure of the filling step. (b) Simulation result of electrostatic adsorption of DNAs to PLL surface. (c) Molecular simulation of DMSO effect: the radial distribution function of P atom of the phosphate group and the sodium ions. The presence of DMSO pumps sodium ions from the 2nd shell to the 1st shell (arrow). (d) Schematics for DMSO effect. Green circles represent sodium ions.

glass substrate occurs when solvent is evaporated (Fig. 3.3). Indeed, the final patterning results after solvent evaporation and cross-linking (Fig. 3.1c, top) reflect the trend established by the aqueous fluorescence images; Scheme 3.2 produces uniform DNA barcodes across the substrate, while Scheme 3.1 does not. Line profiles corresponding to Fig 3.1c. can be found in Fig. 3.4

In order to understand the difference in patterning uniformity between Schemes 3.1 and 3.2, we considered the electrostatic environment for each case. As depicted in Fig. 3.5a, the PDMS side walls carry a slightly negative zeta potential, whereas the PLL surface has a strong positive zeta potential.[32] When the ssDNA solution in Scheme 3.1 is introduced to

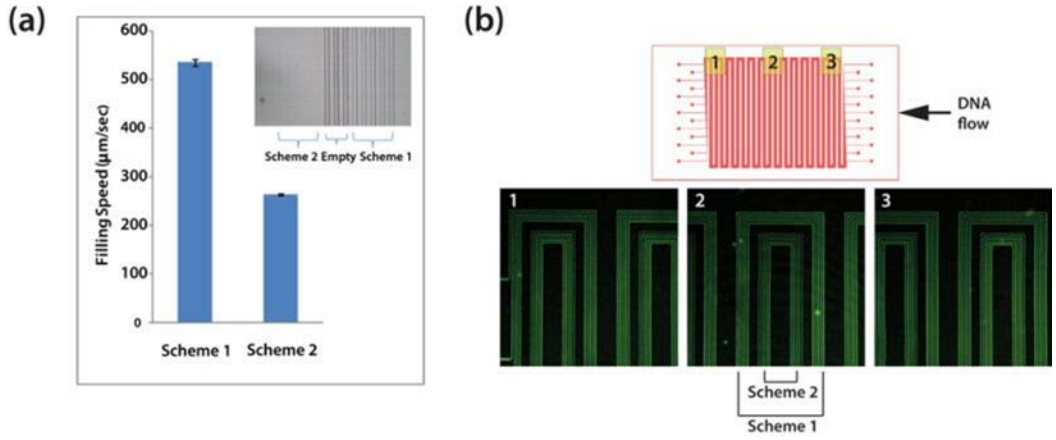

Figure 3.6 Results from experiments designed to more fully understand the effect of electrostatic adsorption of DNA within the microchannels during flow patterning. (a) Measurements of the flow speed of PBS solution of DNA oligomers (Scheme 1) and PBS/DMSO solution (Scheme 2) in the microfluidic channels. The filling process was optically monitored and recorded as a movie. The speed was calculated when the flow makes the fifth turn in the channel. The filling speed for Scheme 2 was less than that of Scheme 1, an observation that is attributable to the differential channel wetting between the two schemes (inset). The wetting of the PBS/DMSO Scheme 2 fluid was significantly better, a factor that minimizes bubble formation in the channel during the drying step. (b) Fluorescence images of DNA patterned within the microchannels of an O_2-plasma-treated bare glass/PDMS device. The highly negative surface induced by plasma treatment minimizes electrostatic adsorption of DNA, resulting in uniform DNA distribution for both Scheme 1 and Scheme 2. The PDMS was solvent extracted just prior to bonding in order to prolong its hydrophilicity following plasma treatment.[14] Panels 1, 2, and 3 represent different locations in the flow patterning device.

the channel, ssDNA near the PLL matrix is electrostatically immobilized, thereby generating a concentration gradient.[23] As the solution flows towards the channel exit, the ssDNA oligomers are continually depleted via deposition onto the PLL surface. Fig. 3.5b shows the results from a rough simulation designed to capture the mean concentration of aqueous ssDNA as the solution traverses a channel. The simulation implies that the effect of electrostatic adsorption proves dominant even at high DNA concentration, a result that agrees well with the observed behavior for Scheme 3.1 in Fig. 3.1b. A detailed description

of the model and assumptions employed can be found in Section 3.2.9. We tested this model via the strong negative charging of all four channel surfaces via O_2 plasma treatment. Consistent with the model, both Scheme 3.1 and Scheme 3.2 exhibited equivalently uniform distribution of fluorescence intensity across the chip (Fig. 3.6b). We note that lack of the positive charges on the bottom surface failed to hold DNAs during the drying procedure and the plasma treatment induces the irreversible bonding of PDMS and glass, which limits further use beyond this experimental test.

Scheme 3.1 and 3.2 results imply that DMSO alleviates the electrostatic adsorption effect. In order to more fully understand this, we performed molecular dynamics (MD) simulations of DNA in PBS and PBS/DMSO solutions; 3 ns of NPT (NPT is a simulation in which moles (N), pressure and temperature are held constant) MD simulations were performed, with the last 1 ns trajectory being employed for analysis. We examined the

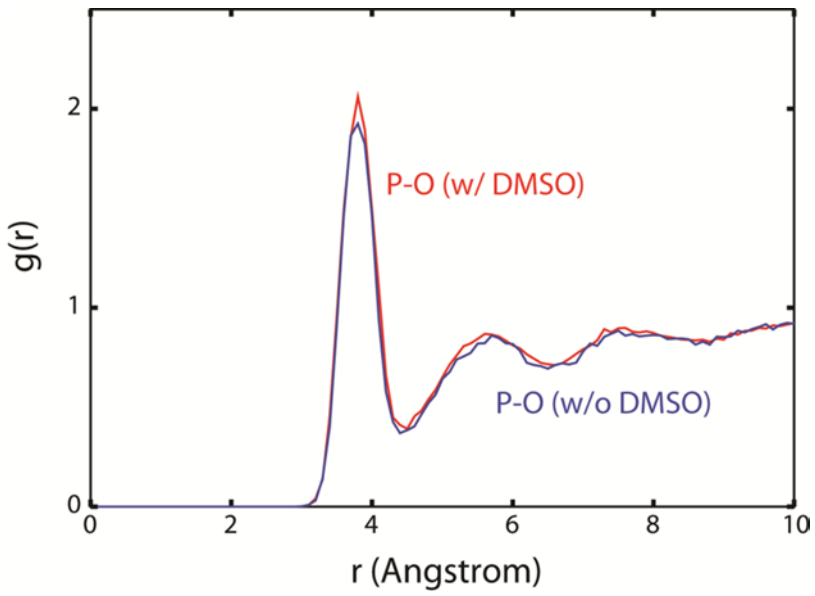

Figure 3.7 Molecular simulation resulting from the influence of DMSO in the Scheme 3.2 process. The radial distribution function of the P atom of the phosphate group of the DNA backbone and O atom of the water molecule is not influenced by the presence of DMSO.

radial distribution function of phosphorous atoms in the DNA backbone with respect to various elements of the surrounding solvent. For example, the radial distribution function of P and the O atom of a water molecule is virtually unperturbed by the addition of DMSO (Fig. 3.7). Consequently, it is unsurprising that the radial distribution function of P and the S atom of DMSO (Fig. 3.5c, black solid line) reveals that DMSO is not forming a solvation structure with the DNA backbone. However, Figure 3.5c demonstrates a clear interaction between P and Na^+ ions which delineates into two well-defined shell structures: the first is located at r<4.3Å while the second is located at 4.3Å<r<6.6Å; these are similar to the locations of the first and the second water solvation structures. By integrating the radial distribution functions, we determined the number of molecules per phosphate in the first and second shells for both PBS and PBS/DMSO solutions. Although the number of H_2Os per shell is virtually independent of DMSO, DMSO does significantly increase the number of Na^+ ions in the first shell (from 0.14 to 0.24), and it decreases the number of Na^+ ions in the second shell (from 0.61 to 0.34). Conversely, the number of DMSO molecules is almost zero in the first shell (0.01) but becomes significant in the second shell (0.20). Thus, we conclude that DMSO, with a lower dielectric constant relative to water (47.2 vs. 80), destabilizes the solvation energy of Na^+ in the second shell. This thermodynamic change prompts the sodium ions to move to the first shell where they are stabilized by electrostatic interactions with the negatively charged phosphate groups. The increased number of sodium ions near the DNA backbone more efficiently screens the negative charges of phosphate groups, thereby reducing electrostatic interactions of the DNA with the PLL surface, resulting in uniform DNA distribution throughout the channels. Although the addition of DMSO to DNA patterning solutions yields the same ultimate effect for both

traditional spotted arrays and microfluidics-patterned barcodes, the underlying mechanisms are completely different. We conclude that Scheme 3.2 is intrinsically superior relative to Scheme 3.1.

We now turn towards analyzing Scheme 3.3, and comparing it against Scheme 3.2. For this scheme, the PAMAM dendrimers are first covalently attached to the aminated glass surface, and then (aminated) ssDNA oligomers are covalently attached to the dendrimers. The lack of a solvent evaporation step makes Scheme 3.3 significantly more rapid than Scheme 3.2. We flowed activated PAMAM dendrimers, followed by aminated ssDNA, through ten microfluidic channels (Fig. 3.1b). Note that the aqueous DNA distribution is expected to be uniform because the substrate surface is comprised of charge-neutral N-hydroxysuccinimide (NHS)-modified carboxylates which minimize electrostatic interactions. The resulting DNA microarray was assayed for uniformity with complementary DNAs labeled with Cy3-fluorophores. Visual analysis indicates good uniformity across the chip (Fig. 3.1c, bottom). In order to quantitate the patterning quality for all three schemes, we obtained signal intensities for each channel at sixteen locations within the patterning region and calculated the coefficient of variation (CV). CV is defined as the standard deviation divided by the mean and expressed as a percentage. CVs for Schemes 3.1, 3.2, and 3.3 registered 69.8%, 10.5%, and 10.9%, respectively. Thus, we conclude that Schemes 3.2 and 3.3 offer consistent DNA loading across the entire substrate.

Having established that Scheme 2 and 3 produce consistent, large-scale DNA barcodes, we then extended our analysis of array consistency to protein measurements. We previously demonstrated that, when using the DEAL platform for multiplex protein sensing in microfluidics channels, the sensitivities of the assays directly correlate with the amount

of immobilized DNA,[15] up to the point where the DNA coverage is saturated. We performed multiple protein assays along the length of our DNA stripes to ensure that the above described results would translate into stable and sensitive barcodes for protein sensing. All protein assays were performed in microfluidic channels that were oriented perpendicular to the patterned barcodes (five channels for Scheme 3.2 and four channels for Scheme 3.3). This allowed us to test distal microarray repeats with a single small analyte volume. For barcodes prepared using Scheme 3.2, we utilized the DEAL technique to convert them into antibody barcodes designed to assay the following proteins: phosphorylated (phospho)-steroid receptor coactivator (Src), phospho-mammalian target of rapamycin (mTOR), phospho-p70 S6 kinase (S6K), phospho-glycogen synthase kinase (GSK)-3α/β, phospho-p38α, phospho-extracellular signal-regulated kinase (ERK), and total epidermal growth factor receptor (EGFR) at 10 ng/ml and 1 ng/ml concentrations. This panel samples key nodes of the phosphoinositide 3-kinase (PI3K) signaling pathway within GBM, and are used below for single-cell assays.[33] For barcodes prepared using Scheme 3.3, we similarly converted the DNA barcodes into antibody barcodes designed to detect the three proteins (interferon (IFN)-γ, tumor necrosis factor (TNF)α, and interleukin (IL)-2) at 100 ng/ml and 10 ng/ml. All the DNAs used were pre-validated for the orthogonality in order to avoid cross-hybridization and the sequences can be found in Table 3.1. The detection scheme is similar to a sandwich immunoassay. Captured proteins from primary antibodies were fluorescently visualized by biotin-labeled secondary antibodies and Cy5-labeled streptavidin. For both cases, data averaged from multiple DNA repeats across the chip yielded CVs that were commensurate with those of the underlying DNA barcodes (from 10 ng/ml concentration, 7% for Scheme 3.2 and 17% for Scheme 3.3, respectively).

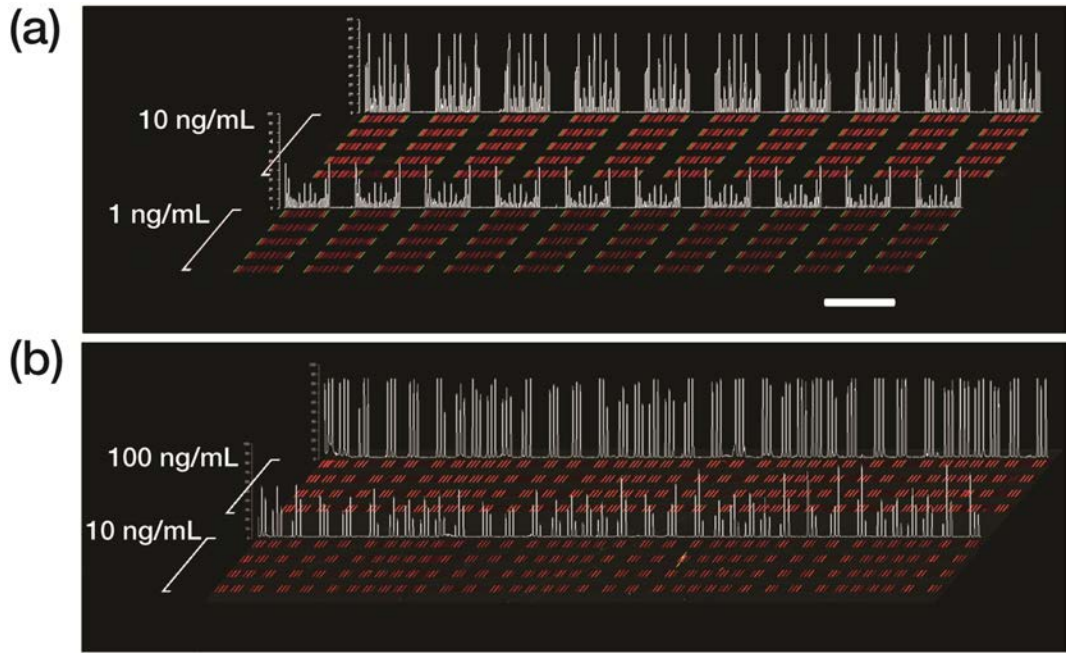

Figure 3.8 Contrast-enhanced raw data extracted from multi-protein calibration experiments performed on a substrate prepared by Scheme 2 (a) and Scheme 3 (b). Each red bar represents a unique protein measurement, and is clustered with up to ten additional proteins (for Scheme 2). The clusters become symmetrical due to the winding nature of the barcode pattern, so that each cluster actually contains two measurements of each protein. Clustering is less evident in (b) because a lower-density barcode pattern was employed. Recombinant proteins were analyzed across five discrete channels per concentration for (a) and four discrete channels per concentration for (b); quantitative data for statistical analysis was extracted from all the repeats in each of the channels. By utilizing identical DEAL cocktails followed by identical standard protein cocktails, the reproducibility was also checked. The identical signal patterns within individual channels and between channels of similar concentrations demonstrate the good uniformity and quality of DNA barcodes. Signal intensity profiles sampled from one analysis channel per concentration are quantified in white. Scale bar: 2 mm

Fig. 3.8 shows line profiles of the signal intensities along with the raw data, and demonstrate a better uniformity for barcodes prepared according to Scheme 3.2. While we found that Scheme 3.3 could produce barcodes that were close in quality to those of Scheme 3.2, the absolute (chip-to-chip) consistency of Scheme 3.3 is hard to guarantee due to its use of the unstable coupling reagents 1-ethyl-3-(3-dimethylaminopropyl)

carbodiimide (EDC) and NHS.[34] Moreover, although Scheme 3.3 is faster, the detailed procedure itself is more labor intensive; Scheme 3.2 can potentially be automated. Thus, we chose Scheme 3.2 as the preferred barcode patterning method. With Scheme 3.2, over 90% of the patterned slides showed good quality for the test.

We validated the use of the antibody barcodes by applying them towards the multiplex assay of cytoplasmic proteins from single cells. There is a significant body of evidence which demonstrates that genetically identical cells can exhibit significant functional heterogeneity—behavior that cannot be captured by proteomics techniques that average data across a population.[35] We therefore designed a highly parallel microfluidic device capable of isolating single/few numbers of cells in chambers with a full complement of antibody barcodes designed to detect intracellular proteins (Fig. 3.2). Fig. 3.9a shows a schematic of the device and the DEAL-based protein detection scheme. The small chamber size keeps the finite number of protein molecules concentrated, thereby enhancing sensitivity. Assaying such a panel of proteins would not be possible without a high-density antibody array, such as the barcodes utilized here, for the following reasons: First, all the barcodes should fit into such a small chamber for multiplexing. Second, since data averaging in such a spatially-constrained scheme is impractical, it is critical to have consistent DNA loading across the microrarray if data comparisons are to be meaningful.

We chose the U87 GBM cell line as a model system for our platform. GBM is the most common malignant brain tumor found in adults, and is the most lethal of all cancers. As the name implies, GBM exhibits extensive biological variability and heterogeneous clinical behavior.[36] EGFR is an important GBM oncogene and therapeutic target.[37] Thus, we assayed for eleven intracellular proteins associated with the EGFR-activated PI3K

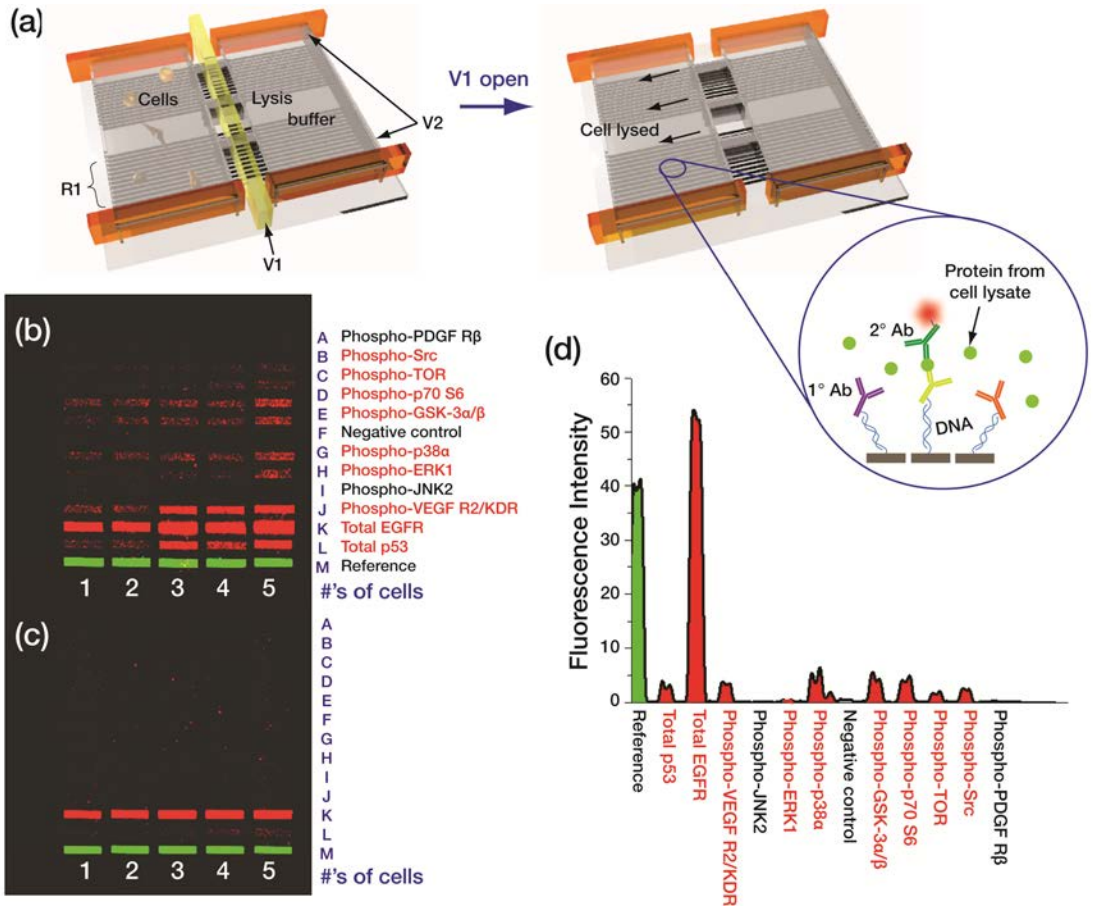

Figure 3.9 (a) A schematic representation of the single-cell, intracellular protein analysis device. Single or few cells are incubated in an isolated chamber under varying stimuli. Intracellular proteins are assayed by introducing a pre-aliquoted lysis buffer, whereupon the released proteins bind to the DEAL (DNA-labeled antibody) barcode within the chamber. V1: valve for lysis buffer control, V2: valve for isolated chamber formation, and R1: DNA barcode array converted into DEAL antibody array. (b) Contrast-enhanced images of developed barcode assays highlight the benefits of using Scheme 2 (b) vs. Scheme 3.1 (c). Protein names listed in red font correspond to those which were detected using Scheme 3.2 barcodes. (d) Representative fluorescence intensity profile from the single cell lysate of (b)

signaling pathway. We provide representative sets of data for protein detection from the lysate of 1 to 5 cells (Fig. 3.9b and 3.9c). Eight proteins were detected from single-cell lysate and up to nine proteins were detected from five cells when using barcodes patterned by Scheme 3.2 (Fig. 3.9b and Fig. 3.9d), whereas only one protein could be detected from

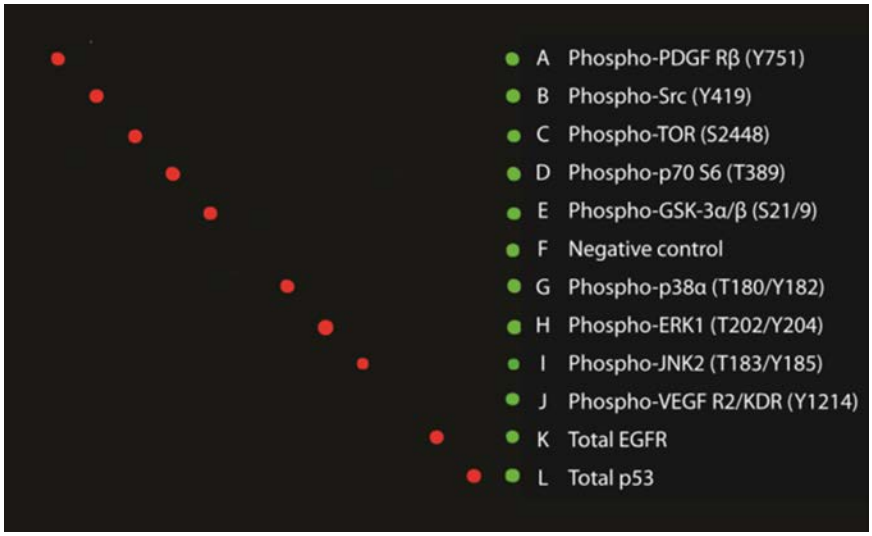

Figure 3.10 Antibody cross-reactivity tests. All antibodies were pre-selected based on such cross-reactivity tests. A pin-spotted DNA microarray was used for a DEAL-based protein detection approach—similar to the assays used within the SCBC microfluidic devices for single-cell proteomics. Each row shows the results from different conditions. For all conditions, the same cocktail of DEAL conjugates was used, and included one conjugate for each of the 11 proteins assayed. For each row, only one target recombinant protein was tested. The target proteins were introduced at concentrations between 5–50 ng/mL, depending on the sensitivity of each antibody pair. Red spots are signals from the target proteins and the green spots are reference signals from Cy3-labeled DNA sequence M‘. Phospho-VEGFR2 was not validated because the recombinant protein is not commercially available.

barcodes prepared by Scheme 3.1 (Fig. 3.9c). All the separate protein assays were screened for cross-reactivity (Fig. 3.10), and, for the cases where recombinant proteins were available, quantitation curves for each protein assay were measured (Fig 3.11). More detailed statistical analysis of these cells, as well as genetic variants thereof, is currently being investigated.

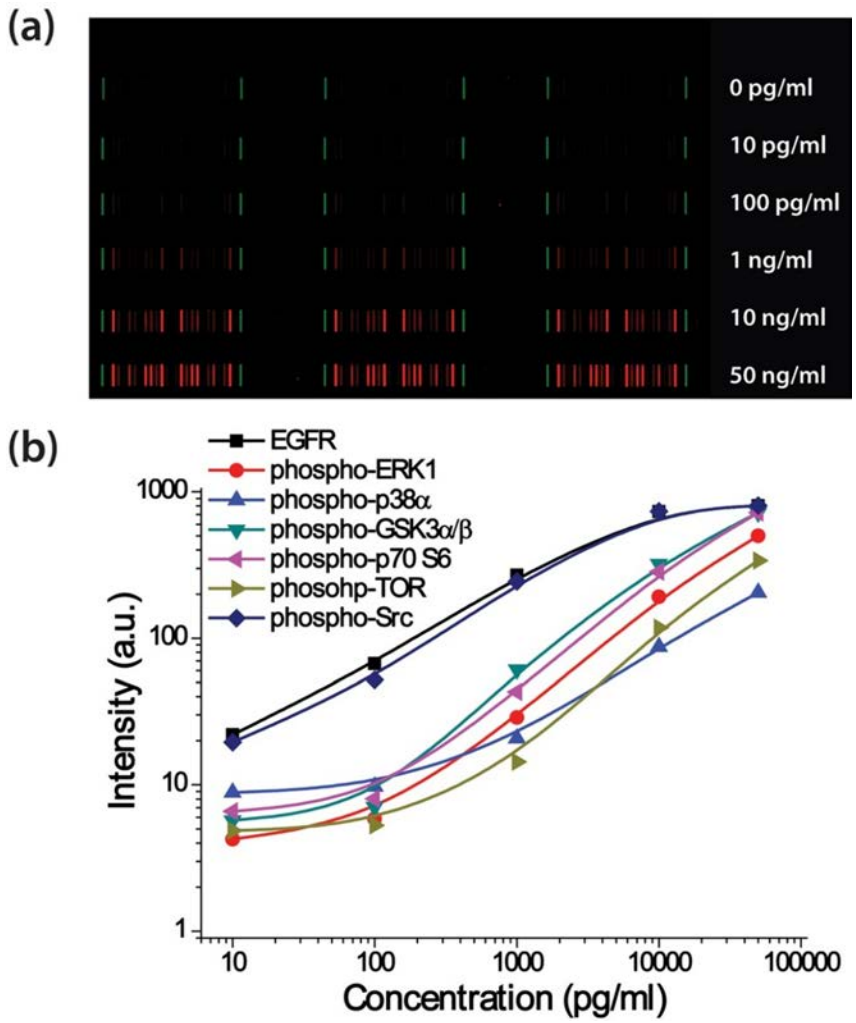

Figure 3.11 Calibration data for proteins in the panel. (a) Representative scanned images showing serial dilution measurements of selected proteins. Recombinant proteins were serially diluted (50 ng/mL, 10 ng/mL, 1 ng/mL, 100 pg/mL, 10 pg/mL, and 0 pg/mL) in 1X PBS and flowed into the different microchannels of the microfluidic device for cell lysis analysis. Valves were immediately closed to compartmentalize standard proteins into microchambers followed by on-chip lysis buffer diffusion on ice for 2 hr. (b) Calibration curves of EGFR, p-ERK, p-p38α, p-GSK3α/β, p-p70S6K, p-mTOR, and p-Src are plotted based on the results from a) to demonstrate the quantitative characteristics of the analysis. The sensitivities identified from the calibration curves are similar to standard ELISA sensitivities (e.g., EGFR: ~ 10 pg/mL, p-p70S6K: ~ 100 pg/mL, p-mTOR: ~ 200 pg/mL).

3.4 Conclusions

We have identified a protocol for generating high-quality, high-density DNA barcode patterns by comparing three microfluidics-based patterning schemes. We find, through both experiment and theory, that the electrostatic attractions between positively charged PLL substrates and the negatively-charged DNA backbone induces significant non-uniformity in the patterning process, but that those electrostatic interactions may be mediated by adding DMSO to the solution, resulting in uniform and highly reproducible barcodes patterned using ~ 55-cm-long channels that template barcodes across an entire 2.5-cm-wide glass slide. Dendrimer-based covalent immobilization also yields good ultimate uniformity, but is hampered by a relatively unstable chemistry that limits run-to-run reproducibility. DNA barcodes were coupled with the DEAL technique to generate antibody barcodes, and then integrated into specifically designed microfluidic chips for assaying cytoplasm proteins from single and few lysed U87 model cancer cells. Successful detection of a panel of such proteins represents the potential of our platform to be applied to various biological and, perhaps, clinical applications.

3.5 References

1. Heath, J. R.; Davis, M. E., Nanotechnology and cancer. *Annual Review of Medicine* **2008**, 59, 251–265.
2. Heath, J. R.; Phelps, M. E.; Hood, L., NanoSystems biology. *Molecular Imaging and Biology* **2003**, 5, (5), 312–325.

3. Khalil, I. G.; Hill, C., Systems biology for cancer. *Current Opinion in Oncology* **2005**, 17, (1), 44–48.
4. Zheng, G.; Patolsky, F.; Cui, Y.; Wang, W. U.; Lieber, C. M., Multiplexed electrical detection of cancer markers with nanowire sensor arrays. *Nature Biotechnology* **2005**, 23, (10), 1294–1301.
5. Niemeyer, C. M., Functional devices from DNA and proteins. *Nano Today* **2007**, 2, (2), 42–52.
6. Boozer, C.; Ladd, J.; Chen, S.; Jiang, S., DNA-directed protein immobilization for simultaneous detection of multiple analytes by surface plasmon resonance biosensor. *Analytical Chemistry* **2006**, 78, (5), 1515–1519.
7. Wacker, R.; Niemeyer, C. M., DDI-microFIA—A readily configurable microarray-fluorescence immunoassay based on DNA-directed immobilization of proteins. *Chembiochem* **2004**, 5, (4), 453–459.
8. Schroeder, H.; Adler, M.; Gerigk, K.; Muller-Chorus, B.; Gotz, F.; Niemeyer, C. M., User configurable microfluidic device for multiplexed immunoassays based on DNA-directed assembly. *Analytical Chemistry* **2009**, 81, (3), 1275–1279.
9. Wacker, R.; Schröder, H.; Niemeyer, C. M., Performance of antibody microarrays fabricated by either DNA-directed immobilization, direct spotting, or streptavidin-biotin attachment: a comparative study. *Analytical Biochemistry* **2004**, 330, (2), 281–287.
10. Douglas, E. S.; Chandra, R. A.; Bertozzi, C. R.; Mathies, R. A.; Francis, M. B., Self-assembled cellular microarrays patterned using DNA barcodes. *Lab on a chip* **2007**, 7, (11), 1442–1448.

11. Bailey, R. C.; Kwong, G. A.; Radu, C. G.; Witte, O. N.; Heath, J. R., DNA-encoded antibody libraries: a unified platform for multiplexed cell sorting and detection of genes and proteins. *Journal of the American Chemical Society* **2007**, 129, (7), 1959–1967.
12. Niemeyer, C. M.; Sano, T.; Smith, C. L.; Cantor, C. R., Oligonucleotide-Directed Self-Assembly of Proteins—Semisynthetic DNA Streptavidin Hybrid Molecules as Connectors for the Generation of Macroscopic Arrays and the Construction of Supramolecular Bioconjugates. *Nucleic Acids Research* **1994**, 22, (25), 5530–5539.
13. Sano, T.; Smith, C.; Cantor, C., Immuno-PCR: very sensitive antigen detection by means of specific antibody-DNA conjugates. *Science* **1992**, 258, (5079), 120–122.
14. Vickers, J. A.; Caulum, M. M.; Henry, C. S., Generation of Hydrophilic Poly(dimethylsiloxane) for High-Performance Microchip Electrophoresis. *Analytical Chemistry* **2006**, 78, (21), 7446–7452.
15. Fan, R.; Vermesh, O.; Srivastava, A.; Yen, B. K.; Qin, L.; Ahmad, H.; Kwong, G. A.; Liu, C. C.; Gould, J.; Hood, L.; Heath, J. R., Integrated barcode chips for rapid, multiplexed analysis of proteins in microliter quantities of blood. *Nature Biotechnology* **2008**, 26, (12), 1373–1378.
16. Thorsen, T.; Maerkl, S. J.; Quake, S. R., Microfluidic large-scale integration. *Science* **2002**, 298, (5593), 580–584.
17. Duan, Y.; Wu, C.; Chowdhury, S.; Lee, M. C.; Xiong, G.; Zhang, W.; Yang, R.; Cieplak, P.; Luo, R.; Lee, T.; Caldwell, J.; Wang, J.; Kollman, P., A point-charge force field for molecular mechanics simulations of proteins based on condensed-phase quantum mechanical calculations. *Journal of Computational Chemistry* **2003**, 24, (16), 1999–2012.

18. Cornell, W. D.; Cieplak, P.; Bayly, C. I.; Gould, I. R.; Merz, K. M.; Ferguson, D. M.; Spellmeyer, D. C.; Fox, T.; Caldwell, J. W.; Kollman, P. A., A Second Generation Force Field for the Simulation of Proteins, Nucleic Acids, and Organic Molecules. *Journal of the American Chemical Society* **1995**, 117, (19), 5179–5197.

19. Plimpton, S., Fast Parallel Algorithms for Short-Range Molecular Dynamics. *Journal of Computational Physics* **1995**, 117, (1), 1–19.

20. Tung, C. S.; Carter, E. S., 2nd, Nucleic acid modeling tool (NAMOT): an interactive graphic tool for modeling nucleic acid structures. *Computer Applications in the Biosciences* **1994**, 10, (4), 427–433.

21. Jorgensen, W. L.; Chandrasekhar, J.; Madura, J. D.; Impey, R. W.; Klein, M. L., Comparison of Simple Potential Functions for Simulating Liquid Water. *Journal of Chemical Physics* **1983**, 79, (2), 926–935.

22. Hockney, R. W.; Eastwood, J. W., Computer Simulation Using Particles. *McGraw-Hill: New York*, **1981**.

23. Benn, J. A.; Hu, J.; Hogan, B. J.; Fry, R. C.; Samson, L. D.; Thorsen, T., Comparative modeling and analysis of microfluidic and conventional DNA microarrays. *Analytical Biochemistry* **2006**, 348, (2), 284–293.

24. Tinland, B.; Pluen, A.; Sturm, J.; Weill, G., Persistence Length of Single-Stranded DNA. *Macromolecules* **1997**, 30, (19), 5763–5765.

25. Nkodo, A. E.; Garnier, J. M.; Tinland, B.; Ren, H.; Desruisseaux, C.; McCormick, L. C.; Drouin, G.; Slater, G. W., Diffusion coefficient of DNA molecules during free solution electrophoresis. *Electrophoresis* **2001**, 22, (12), 2424–2432.

26. Dufva, M., Fabrication of high quality microarrays. *Biomolecular Engineering* **2005**, 22, (5–6), 173–184.

27. Le Berre, V.; Trevisiol, E.; Dagkessamanskaia, A.; Sokol, S.; Caminade, A. M.; Majoral, J. P.; Meunier, B.; Francois, J., Dendrimeric coating of glass slides for sensitive DNA microarrays analysis. *Nucleic Acids Re*search **2003**, 31, (16), e88.

28. Bosman, A. W.; Janssen, H. M.; Meijer, E. W., About Dendrimers: Structure, Physical Properties, and Applications. *Chemical Reviews* **1999**, 99, (7), 1665–1688.

29. Benters, R.; Niemeyer, C. M.; Drutschmann, D.; Blohm, D.; Wohrle, D., DNA microarrays with PAMAM dendritic linker systems. *Nucleic Acids Research* **2002**, 30, (2), E10.

30. Angenendt, P.; Glokler, J.; Sobek, J.; Lehrach, H.; Cahill, D. J., Next generation of protein microarray support materials: evaluation for protein and antibody microarray applications. *Journal of Chromatogrphy A* **2003**, 1009, (1–2), 97–104.

31. Ajikumar, P. K.; Ng, J. K.; Tang, Y. C.; Lee, J. Y.; Stephanopoulos, G.; Too, H. P., Carboxyl-terminated dendrimer-coated bioactive interface for protein microarray: high-sensitivity detection of antigen in complex biological samples. *Langmuir* **2007**, 23, (10), 5670–5677.

32. Kuo, A.-T.; Chang, C.-H.; Wei, H.-H., Transient currents in electrolyte displacement by asymmetric electro-osmosis and determination of surface zeta potentials of composite microchannels. *Applied Physics Letters* **2008**, 92, (24), 244102–244103.

33. Network, C. G. A. R., Comprehensive genomic characterization defines human glioblastoma genes and core pathways. *Nature* **2008**, 455, (7216), 1061–1068.

34. Kausaite, A.; Dijk, M. v.; Castrop, J.; Ramanaviciene, A.; Baltrus, J. P.; Acaite, J.; Ramanavicius, A., Surface plasmon resonance label-free monitoring of antibody antigen interactions in real time. *Biochemistry and Molecular Biology Education* **2007**, 35, (1), 57–63.

35. Krutzik, P. O.; Irish, J. M.; Nolan, G. P.; Perez, O. D., Analysis of protein phosphorylation and cellular signaling events by flow cytometry: techniques and clinical applications. *Clinical Immunology* **2004**, 110, (3), 206–221.

36. Liang, Y.; Diehn, M.; Watson, N.; Bollen, A. W.; Aldape, K. D.; Nicholas, M. K.; Lamborn, K. R.; Berger, M. S.; Botstein, D.; Brown, P. O.; Israel, M. A., Gene expression profiling reveals molecularly and clinically distinct subtypes of glioblastoma multiforme. *Proceedings of the National Academy of Sciences of the United States of America* **2005**, 102, (16), 5814–5819.

37. Lee, J. C.; Vivanco, I.; Beroukhim, R.; Huang, J. H. Y.; Feng, W. L.; DeBiasi, R. M.; Yoshimoto, K.; King, J. C.; Nghiemphu, P.; Yuza, Y.; Xu, Q.; Greulich, H.; Thomas, R. K.; Paez, J. G.; Peck, T. C.; Linhart, D. J.; Glatt, K. A.; Getz, G.; Onofrio, R.; Ziaugra, L.; Levine, R. L.; Gabriel, S.; Kawaguchi, T.; O'Neill, K.; Khan, H.; Liau, L. M.; Nelson, S. F.; Rao, P. N.; Mischel, P.; Pieper, R. O.; Cloughesy, T.; Leahy, D. J.; Sellers, W. R.; Sawyers, C. L.; Meyerson, M.; Mellinghoff, I. K., Epidermal growth factor receptor activation in glioblastoma through novel missense mutations in the extracellular domain. *PLoS Medicine* **2006**, 3, (12), e485.